

# Local observation of modes from three-dimensional woodpile photonic crystals with near-field microspectroscopy under supercontinuum illumination

Baohua Jia,<sup>1,3</sup> Andrew H. Norton,<sup>2</sup> Jiafang Li,<sup>1</sup> Adel Rahmani,<sup>2</sup> Ara A. Asatryan,<sup>2</sup> Lindsay C. Botten,<sup>2</sup> and Min Gu<sup>1,\*</sup>

<sup>1</sup>Centre for Micro-Photonics and Centre for Ultrahigh-bandwidth Devices (CUDOS), Faculty of Engineering and Industrial Sciences, Swinburne University of Technology, P.O. Box 218, Hawthorn, 3122 Victoria, Australia

<sup>2</sup>Department of Mathematical Sciences and Centre for Ultrahigh-bandwidth Devices (CUDOS), University of Technology, Sydney, Australia

<sup>3</sup>E-mail: [bjia@swin.edu.au](mailto:bjia@swin.edu.au)

\*Corresponding author: [mgu@swin.edu.au](mailto:mgu@swin.edu.au)

Received February 22, 2008; revised April 5, 2008; accepted April 5, 2008;  
posted April 14, 2008 (Doc. ID 92856); published May 13, 2008

A near-field microscope coupled with a near-infrared (NIR) supercontinuum source is developed and applied to characterize optical modes in a three-dimensional (3D) woodpile photonic crystal (PC) possessing a NIR partial bandgap. Spatially resolved near-field intensity distributions under different illumination wavelengths demonstrate that the electric fields preferentially dwell in the polymer rods or in the gaps between rods, respectively, for frequencies below or above the stop gap, as predicted by the 3D finite-difference time-domain modeling. Near-field microspectroscopy further reveals that the position-dependent band-edge effect plays an important role in PC-based all-optical integrated devices. © 2008 Optical Society of America  
OCIS codes: 050.6624, 050.5298, 180.4243, 300.0300.

Three-dimensional (3D) photonic crystals (PCs) have received increasing attention nowadays because of their capability of controlling and manipulating the flow of light on a microscopic length scale in all dimensions [1]. The band structures and bandgap properties of 3D PCs have been investigated for 3D integrated optical devices including superprisms [2,3], self-collimators [4], slow-light generators [5], waveguides [6], and radiation emission controllers [1,7,8]. In those devices mode distributions and their relation to the bandgap property near the surface of the 3D PCs play an important role. However, spectroscopy and imaging methods based on conventional far-field optics, such as Fourier-transform infrared spectroscopy (FTIR), cannot reveal the subwavelength scale localized mode distributions in 3D PCs. Because of its ability of spatially resolving signals beyond the diffraction limit, scanning near-field optical microscopy (SNOM) has been widely applied to study the local bandgap properties of two-dimensional (2D) PCs [9–11].

Recently, SNOM has also been adopted to investigate 3D PCs [12–14]. However, these studies were not performed at the telecommunication wavelength region nor were band-edge effects fully explored owing to the lack of a bright broadband near-infrared (NIR) source. In this Letter, we present a near-field microspectroscopic system coupled with a NIR supercontinuum source. The system is used to characterize localized optical modes in 3D polymeric woodpile PCs. It has been found experimentally that the electric fields are preferentially located, respectively, in the polymer rods or in the gaps between the rods for

frequencies below or above the stop gap, which is confirmed by the 3D finite-difference time-domain (FDTD) simulation.

The near-field microspectroscopic setup is based on a SNOM system (Solver, NT-MDT) operating in the collection mode [Fig. 1(a)]. A tiny aperture (60 nm on average) at the apex of the coated fiber tip enables subdiffraction resolution. The tip was controlled in close vicinity ( $\sim 10$  nm) to the sample surface by a shear-force feedback system. For NIR microspectroscopic measurement, a beam from an ultrafast laser (Mira, Coherent) was coupled into a single-mode polarization-maintaining PC fiber (PCF, Crystal-Fiber) [Fig. 1(a)]. The cross section of the PCF and the corresponding single-mode hexagonal output from the PCF are shown in the inset of Fig. 1(b). Ow-

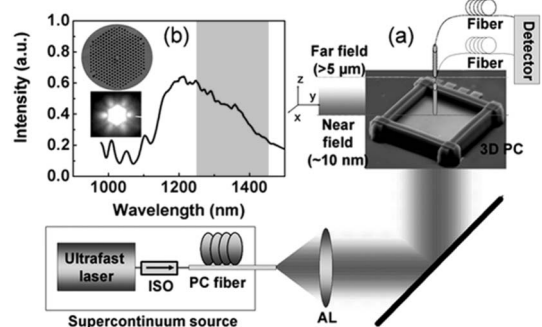


Fig. 1. (a) Setup for supercontinuum generation and coupling into a SNOM. ISO: isolator; AL: achromatic lens. (b) Supercontinuum spectrum. The top inset is a SEM image of the cross section of the PCF. The bottom inset is the mode output of the supercontinuum.

ing to the nonlinear interaction between the femto-second pulses and the PCF [15], supercontinuum radiation spanning from 500 to 1700 nm was produced [Fig. 1(b), the visible part of the spectrum is not shown]. The supercontinuum beam was collimated by an achromatic lens and used to illuminate a 3D PC in the  $\Gamma$ - $X$  direction [Fig. 1(a)].

The woodpile PC investigated under the near-field microspectroscopic system was fabricated by the two-photon polymerization method [16–18]. A scanning electron microscopy (SEM) image of the PC is presented in the inset of Fig. 2(a). The woodpile lattice has a face-centered cubic (fcc) symmetry with an in-plane lattice constant of 900 nm and a rod thickness of 150 nm. A transmission spectrum of the PC measured with a FTIR spectrometer (Thermo Nicolet) in the  $\Gamma$ - $X$  direction (i.e., the woodpile stacking direction) is displayed in Fig. 2(a), which corresponds to the shadow region of the supercontinuum spectrum in Fig. 1(b). A partial bandgap centered at a wavelength of  $1.34 \mu\text{m}$  (corresponding to a frequency of  $0.746 \mu\text{m}^{-1}$ ) with more than 85% transmission suppression can be clearly identified, agreeing well with the predicted stop gap calculated using the MIT Photonic Bands (MPB) software [19] [Fig. 2(b)]. To model the mode structure above the PC we undertook a 3D FDTD simulation of the woodpile [20]. In the simulation, a normally incident plane wave source was utilized and the power flux through the PC and all field components were monitored. Figures 2(c) and 2(d) show the near-field maps of the electric field intensity over  $3 \times 3$  lattice periods, recorded at frequencies below and above the stop gap, respectively. As expected, the modes are concentrated either in the polymer rods [Fig. 2(c)] or in the gaps [Fig. 2(d)] when the frequency falls into the lower or higher energy band edges.

To demonstrate the mode localization we simultaneously recorded the topographic image and the optical near-field signals of the 3D PC using the SNOM allowing for an accurate correlation between them. Figure 3(a) shows a topographic image of the PC. The rods in both the first and second layers are clearly evident with fine surface features demonstrating a high spatial resolution. The spectrum-integrated near-field optical images acquired by a NIR photomultiplier (Hamamatsu) is presented in Fig. 3(b). A comparison of Figs. 3(a) and 3(b) shows that the bright regions in Fig. 3(b) correspond to the gaps between the rods, suggesting that the higher-frequency components are dominant as predicted by the theoretical result shown in Fig. 2(d). The result is understandable because the supercontinuum spectrum exhibits a higher intensity in the higher-frequency region [from 1200 to 1500 nm as shown in Fig. 1(b)]. When the probe is withdrawn to the far-field region ( $2 \mu\text{m}$  from the PC), apart from a significant decrease in the peak intensity, the contrast diminishes and the optical image (not shown) eventually becomes featureless since the evanescent components vanish.

To further verify the mode localization at different frequencies, near-field images at the higher- [1280 nm, H in Fig. 2(a)] and lower-energy band

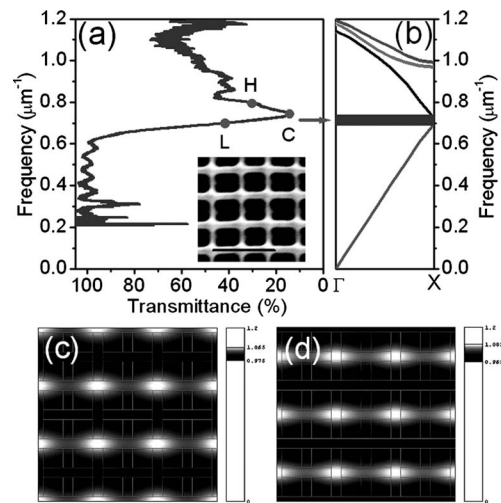


Fig. 2. (a) Transmission spectrum of the woodpile PC. Inset, a SEM image of the PC. Scale bar  $2 \mu\text{m}$ . (b) The calculated band diagram, showing a stop gap in the  $\Gamma$ - $X$  direction. (c), (d) Calculated electric field intensity in a plane perpendicular to the  $\Gamma$ - $X$  direction on (c) the lower- and (d) higher-energy band edges.

edges [1420 nm, L in Fig. 2(a)] and the center of the stop gap (1340 nm) were obtained by utilizing narrow bandpass (10 nm) filters. Figures 3(c) and 3(d) show the acquired normalized near-field intensity distributions. As expected, at the higher-energy band edge [Fig. 3(c)], a high contrast approaching unity is achieved demonstrating the good confinement of the modes in the gaps between the rods. Bright regions in Fig. 3(c) (e.g., the region marked by the square) are observed when the gaps of the first layer overlap those in the second layer. Intensity minima appear (e.g., the region marked by the circle) when the rods in the first layer overlap those in the second layer. In contrast, at the lower-energy band edge [Fig. 3(d)], the optical modes are preferentially confined to the polymer rods. These observations match well the FDTD calculations shown in Figs. 2(c) and 2(d).

The fact that the localized mode patterns dramatically change with frequency illustrates that local spectroscopy would yield spectra that are qualitatively different from the averaged far-field detection [11]. Such local spectra are important to the coupling

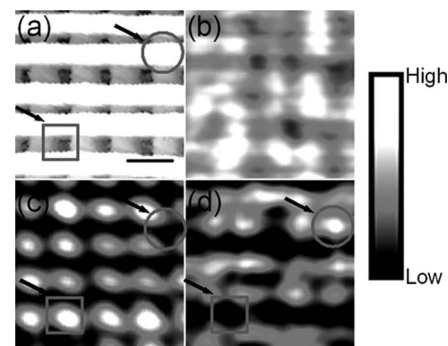


Fig. 3. (a) Topographic image of the PC. Scale bar  $1 \mu\text{m}$ . (b)–(d) Near-field images taken when (b) the supercontinuum illumination was utilized and (c), (d) illumination wavelengths fall into the higher (H)- and lower (L)- energy band edges, respectively.

condition of the integrated devices [1–8]. To obtain the position-dependent transmission spectra, spatially resolved spectroscopy was conducted by the SNOM system in the near-field region at five different lateral positions covering 2.5 lattice periods [points a to e in the inset of Fig. 4(a)] by utilizing a spectrograph in conjugation with an InGaAs detector. To compare, the far-field spectra at these five points were also recorded by the SNOM. The obtained normalized spectra at points a and b are presented in Fig. 4(b). As expected, the far-field transmission spectra at the five positions are almost identical, which means that they are position independent. A stop gap at wavelength 1345 nm was found, matching well that measured with a FTIR.

It is interesting to notice in Fig. 4(b) that the near-field spectra reveal new features that are not shown in the far-field measurement. First of all, owing to the probe tunneling the nonpropagating fields confined within the PC, an increase of 5% to 10% in the transmission at the center of the stop gaps is found. Second, in the local spectrum measured at point a, a bump is observed in the higher-energy band edge [marked by the arrows in Fig. 4(b)] indicating the higher-frequency components are dominant at this point. In the spectrum recorded at point b, where a polymer rod is located, an intensity increase is found at the lower-energy band edge. Similar features were observed in the near-field spectra recorded at the points c, d, and e. As expected, the detected

intensities of all five points at wavelengths  $L$  and  $H$  show clear periodic features as shown in Fig. 4(a).

In conclusion, a near-field microspectroscopy illuminated by a supercontinuum source has been applied to characterize the NIR spectral properties of a 3D woodpile PC. The local optical modes at air bands and dielectric bands of the PC have been observed by spatially and spectrally resolved near-field imaging demonstrating an agreement with the 3D FDTD calculations. The localized spectra exhibit a position-dependent band-edge effect, which is crucially important for efficient coupling in 3D PC-based device designs [2–8].

This work was produced with the assistance of the Australian Research Council (ARC) under its Centers of Excellence program and the Australian Partnership for Advanced Computing (APAC) under its Merit Allocation Scheme. The Centre for Ultrahigh-bandwidth Devices for Optical Systems (CUDOS) is an ARC Centre of Excellence.

## References

1. S. Noda, *J. Lightwave Technol.* **24**, 4554 (2006).
2. J. Serbin and M. Gu, *Adv. Mater. (Weinheim, Ger.)* **18**, 221 (2006).
3. J. Serbin and M. Gu, *Opt. Express* **14**, 3563 (2006).
4. Z. Lu, S. Shi, J. A. Murakowski, G. J. Schneider, C. A. Schuetz, and D. W. Prather, *Phys. Rev. Lett.* **96**, 173902 (2006).
5. K. Sakoda, K. Ohtaka, and T. Ueta, *Opt. Express* **4**, 481 (1999).
6. P. Lodahl, A. F. Van Driel, I. S. Nikolaev, A. Irman, K. Overgaag, D. Vanmaekelbergh, and W. L. Vos, *Nature* **430**, 654 (2004).
7. J. Li, B. Jia, G. Zhou, J. Serbin, C. Bullen, and M. Gu, *Adv. Mater. (Weinheim, Ger.)* **19**, 3276 (2007).
8. J. Li, B. Jia, G. Zhou, and M. Gu, *Appl. Phys. Lett.* **91**, 254101 (2007).
9. A. L. Campillo, J. W. P. Hsu, C. A. White, and A. Rosenberg, *J. Appl. Phys.* **89**, 2801 (2001).
10. H. Gersen, T. J. Karle, R. J. P. Engelen, W. Bogaerts, J. P. Korterik, N. F. Van Hulst, T. F. Krauss, and L. Kuipers, *Phys. Rev. Lett.* **94**, 073903 (2005).
11. N. Louvion, D. Gérard, J. Mouette, F. de Fornel, C. Seassal, X. Letartre, A. Rahmani, and S. Callard, *Phys. Rev. Lett.* **94**, 113907 (2005).
12. E. Fluck, N. F. Van Hulst, W. L. Vos, and L. Kuipers, *Phys. Rev. E* **68**, 156011 (2003).
13. J. Li, B. Jia, G. Zhou, and M. Gu, *Opt. Express* **14**, 10740 (2006).
14. R.-J. Liu, Z.-Y. Li, F. Zhou, and D.-Z. Zhang, *Opt. Express* **15**, 15531 (2007).
15. J. M. Dudley, G. Genty, and S. Coen, *Rev. Mod. Phys.* **78**, 1135 (2006).
16. M. Straub and M. Gu, *Opt. Lett.* **27**, 1824 (2002).
17. B. Jia, J. Li, and M. Gu, *Aust. J. Chem.* **60**, 484 (2007).
18. B. Jia, X. Gan, and M. Gu, *Optik (Jena)* **115**, 358 (2004).
19. S. G. Johnson and J. D. Joannopoulos, MIT Photonic Bands software, <http://ab-initio.mit.edu/mpb>, 1999.
20. A. Taflov and S. C. Hagness, *Computational Electrodynamics: The Finite-Difference Time-Domain Method* (Artech House, 2000).

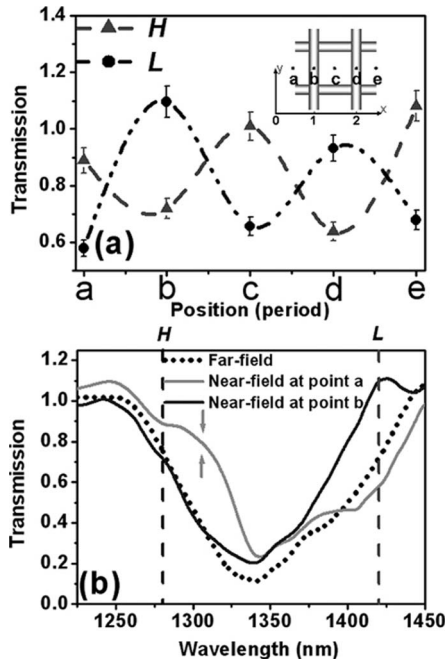


Fig. 4. (a) Normalized near-field intensities at five points a to e (see inset) measured at wavelengths  $L$  and  $H$ . (b) Normalized far- and near-field transmission spectra from the 3D PC measured by a SNOM probe when it was positioned in the gap and polymer rod regions.